

Electronic supplementary information

An interparticle relatively motional DNA walker and its sensing application

Hong Zhang, Xiaowen Xu,* Wei Jiang*

*School of Chemistry and Chemical Engineering, Shandong University, 250100 Jinan, P. R.
China*

Corresponding author: Tel: 86-531-88363888; fax: 86-531-88564464.

*E-mail: xuxw@sdu.edu.cn; wjiang@sdu.edu.cn

Table of Contents

Figure S1. Characterization of synthesized 13nm-AuNPs.....	3
Figure S2. Characterization of the modified amount of WPs and TP-Au13	3
Figure S3. Comparison of fluorescence emission spectra of the interparticle relatively motional DNA walker in the presence of two different concentrations of WP	4
Figure S4. TEM image of the interparticle relatively motional DNA walker consisted of 13 nm WPs (0.2 nM) and 20 nm TPs (1.0 nM) at different reaction time points.	5
Figure S5. UV-Vis absorption spectra of the DNA walker at different operation times.	5
Figure S6. Optimization of the walker operation condition.....	6
Figure S7. Reaction rate of the interparticle relatively motional DNA walker and control conjugate7	
Figure S8. Optimization of the control molecular beacon reaction condition.	8
Figure S9. Optimization of the control nanoprobe reaction condition.....	8
Figure S10. Fluorescence emission spectra of the control molecular beacon (A), control nanoprobe (B) and interparticle relatively motional DNA walker (C)..	9
Figure S11. Schematic diagram of the calculation model.....	10
Figure S12. Characterization of 5nm and 25nm AuNPs.....	12
Figure S13. Characterization of the modified amount of TP-Au5 and TP-Au25	12
Figure S14. DLS characterization of WPs and different sizes of TPs	13
Figure S15. Comparison of anti-interference ability of the interparticle relatively motional DNA walker, control molecular beacon and control nanoprobe.	13
Table S1. Comparison of the DNA walker with some reported strategies for ZIKV related sequence	14
Table S2. Recovery experiment of ZIKV-RNA in human serum	15

Additional figures and discussion.

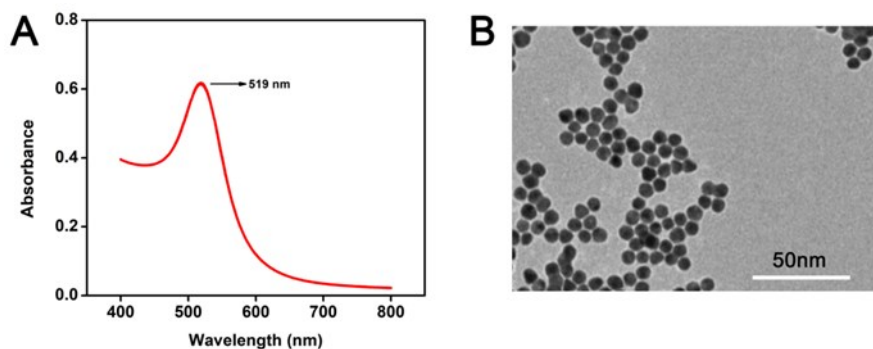


Fig. S1 Characterization of synthesized 13nm-AuNPs. (A) UV-vis absorption spectra and (B) TEM image. The UV spectrum showed that the maximum absorption wavelength of AuNPs was 519 nm, TEM image of AuNPs had uniform spherical particles with particle diameter of about 13 nm. These results indicated that 13nm of AuNPs successfully prepared.

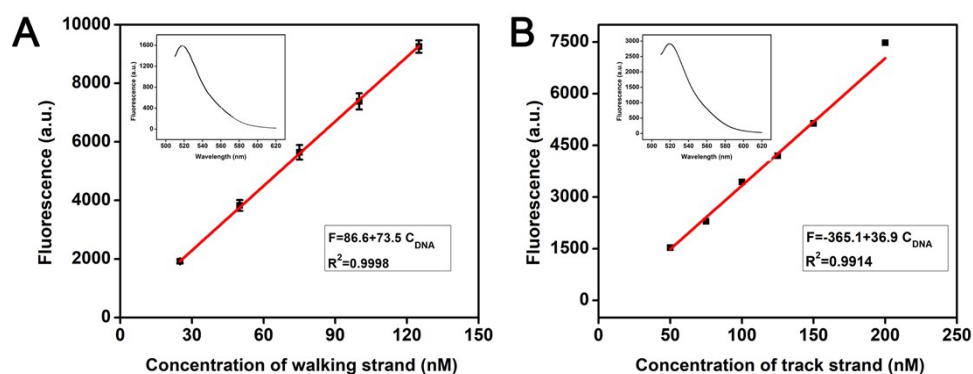


Fig. S2 Characterization of the modified amount of WPs and TP-Au13. (A) Standard linear calibration curves of FAM-labelled walking strand. Inset shows the fluorescence spectra of WPs after incubation with DTT. The Error bars are the standard deviation of three measurement. (B) Standard linear calibration curves of FAM-labelled track strand. Inset shows the fluorescence spectra of TP-Au13 after incubation with DTT.

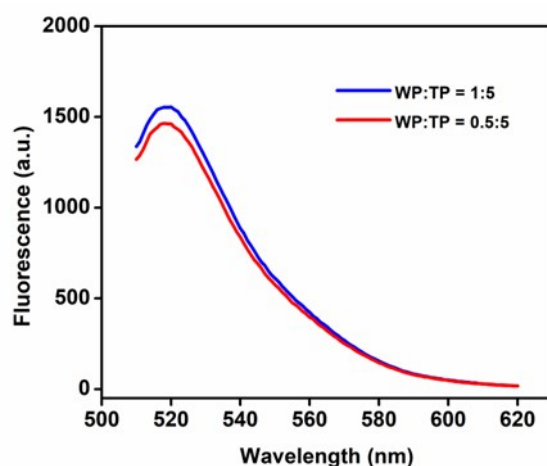


Fig. S3 Comparison of fluorescence emission spectra of the interparticle relatively motional DNA walker in the presence of two different concentrations of WP, while the concentration of TPs is kept at 1.0 nM.

The signal level of the DNA walker in the case of reduced WP concentration is tested. Keeping the same TP concentration, the WP concentration is reduced to be half to characterize DNA walker. After an elongated operation time (6 h) between WP and TP, the fluorescence signal is measured. As shown in Fig. S3, the two types of DNA walkers, with the WP versus TP concentration ratio to be 1:5 and 0.5:5 respectively, finally obtain the similar fluorescence intensity. This suggests the relative motion between WP and TP, which enables that the similar surface area of TP can be interacted by TP even though the concentration of WP is reduced.

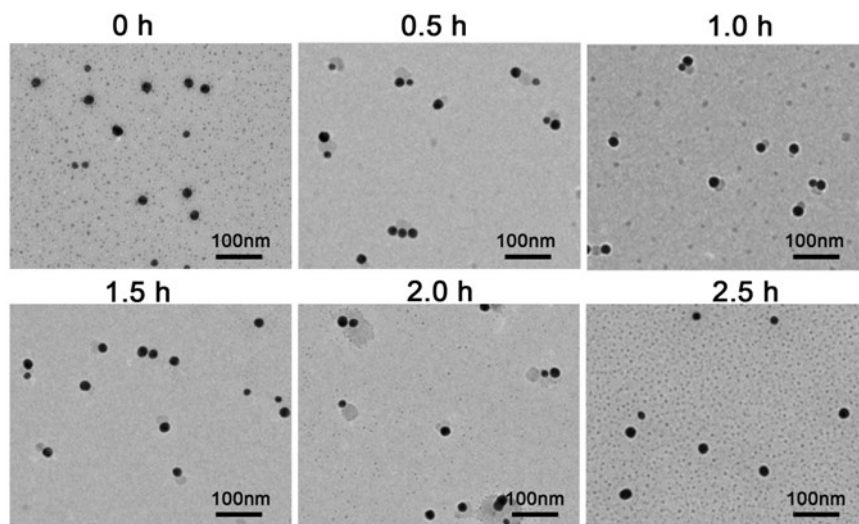


Fig. S4 TEM image of the interparticle relatively motional DNA walker consisted of 13 nm WPs (0.2 nM) and 20 nm TPs (1.0 nM) at different reaction time points.

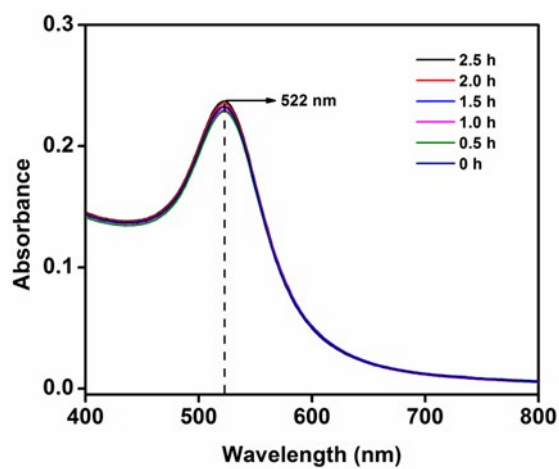


Fig. S5 UV-Vis absorption spectra of the DNA walker at different operation times. The concentration of WPs and TPs are 0.2 nM and 1.0 nM, respectively.

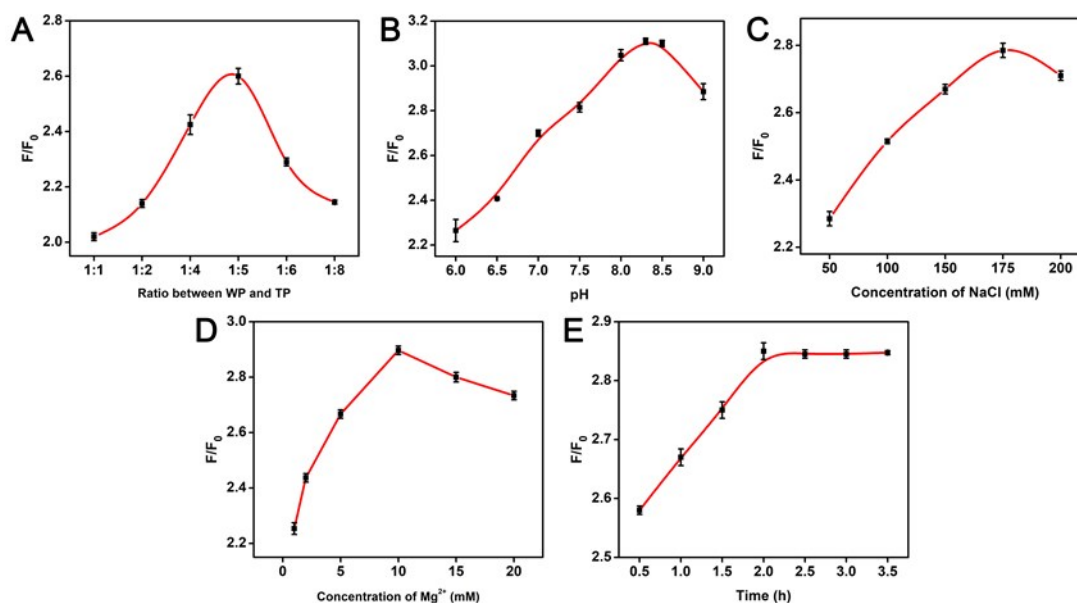


Fig. S6 Optimization of the walker operation condition, in which the curves are drawn based on the spline function method in the Origin software. (A) The influences of different ratios of WPs and TPs on F/F_0 (1:1, 1:2, 1:4, 1:5, 1:6 and 1:8). Conditions: pH = 8.3, [NaCl] = 175 mM, [Mg^{2+}] = 10 mM, operation time of the DNA walker = 2.5 h. (B) Effect of pH conditions on F/F_0 (pH 6.0, 6.5, 7.0, 7.5, 8.0, 8.3, 8.5 and 9.0). Conditions: ratio of WPs to TPs = 1:5, [NaCl] = 175 mM, [Mg^{2+}] = 10 mM, operation time of the DNA walker = 2.5 h. (C) Effect of NaCl concentration on F/F_0 (50, 100, 150, 175 and 200 mM). Conditions: ratio of WPs to TPs = 1:5, pH = 8.3, [Mg^{2+}] = 10 mM, operation time of the DNA walker = 2.5 h. (D) Effect of Mg^{2+} concentration on F/F_0 (1, 2, 5, 10, 15 and 20 mM). Conditions: ratio of WPs to TPs = 1:5, pH = 8.3, [NaCl] = 175 mM, operation time of the DNA walker = 2.5 h. (E) Effect of reaction time on F/F_0 (0.5, 1.0, 1.5, 2.0, 2.5, 3.0 and 3.5 h). Conditions: ratio of WPs to TPs = 1:5, pH = 8.3, [NaCl] = 175 mM, [Mg^{2+}] = 10 mM. The Error bars are the standard deviation of three measurement.

First, in the case of other conditions being optimal, the reaction conditions of the walker were optimized to improve F/F_0 . Cooperative operation performance among DNA walker's components is closely related to the ratio between WPs and TPs, and the appropriate ratio of WPs to TPs is beneficial to improve the binding probability and reduce the potential binding resistance between the WPs and surrounding TPs. As shown in Fig. S6A, when the ratio of WPs to TPs is changed from 1:1 to 1:8, the fluorescence signal increases correspondingly and the value of F/F_0 reaches a maximum at 1:5. Therefore, the ratio of 1:5 is selected as the optimal proportion of WPs to TPs. In addition, since the catalytic activity of DNAzyme is affected by

pH value, we studied the operation of the DNA walker under various pH value conditions. As seen in Fig. S6B, the result indicates that the DNA walker exhibited the best performance at pH 8.3, which is chosen as the optimum pH value for the experiment. The result is in agreement with the fact that the cleavage rate of DNAzyme to substrate is accelerated within a certain alkaline range.^{1,2} The salt concentration mainly affects DNA strand hybridization ability by influencing melting temperature of DNA strand. Consequently, the effect of NaCl concentration on the reaction system is also considered. The result demonstrates that 175 mM NaCl is the appropriate salt concentration of the reaction system (Fig. S6C). Such a salt concentration can promote the hybridization process between WPs and TPs by screening the electrostatic repulsion of AuNPs surfaces. We also investigated the influence of Mg^{2+} concentration toward DNAzyme catalytic activity and obtained that DNAzyme exerts optimal catalytic cleavage activity in 10 mM Mg^{2+} (Fig. S6D), which is selected as the suitable experimental condition. The operation time is essential to performance evaluation of the DNA walker. A largest value of F/F_0 at 2.5 h is observed in Fig. S6E. The operation time of the DNA walker is selected as 2.5 h.

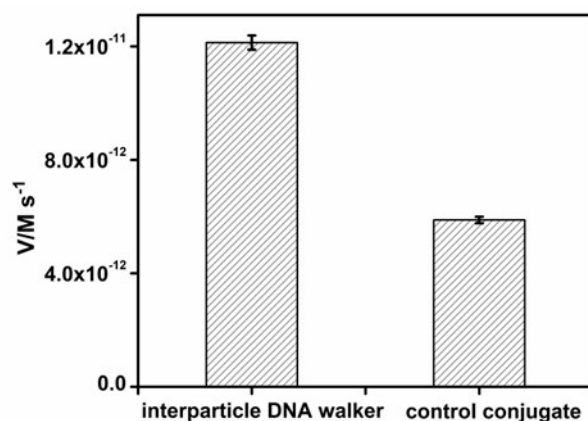


Fig. S7 Reaction rate of the interparticle relatively motional DNA walker and control conjugate in the first 30 min.

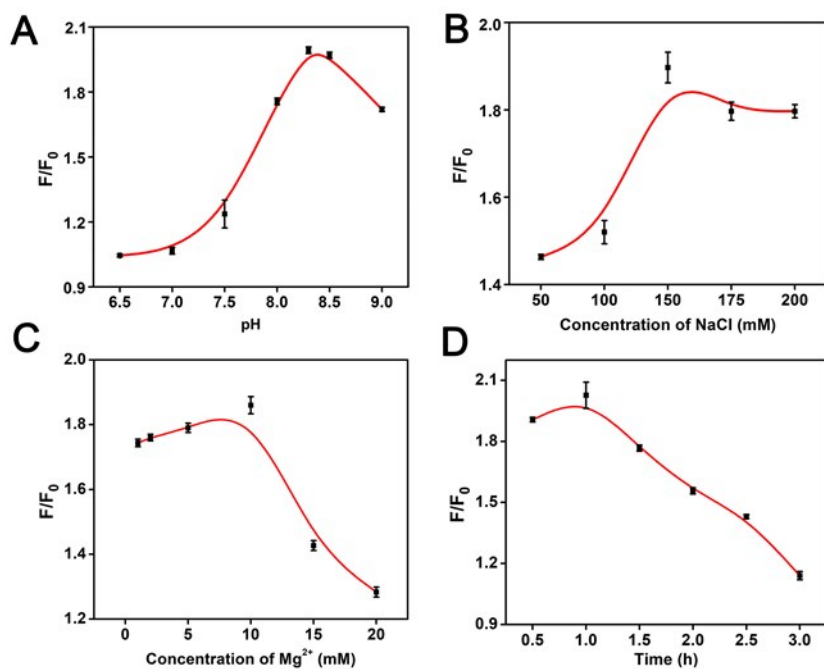


Fig. S8 Optimization of the control molecular beacon reaction condition, in which the curves are drawn based on the spline function method in the Origin software. (A) Effect of pH conditions on F/F_0 . (B) Effect of NaCl concentration on F/F_0 . (C) Effect of Mg^{2+} concentration on F/F_0 . (D) Effect of reaction time on F/F_0 .

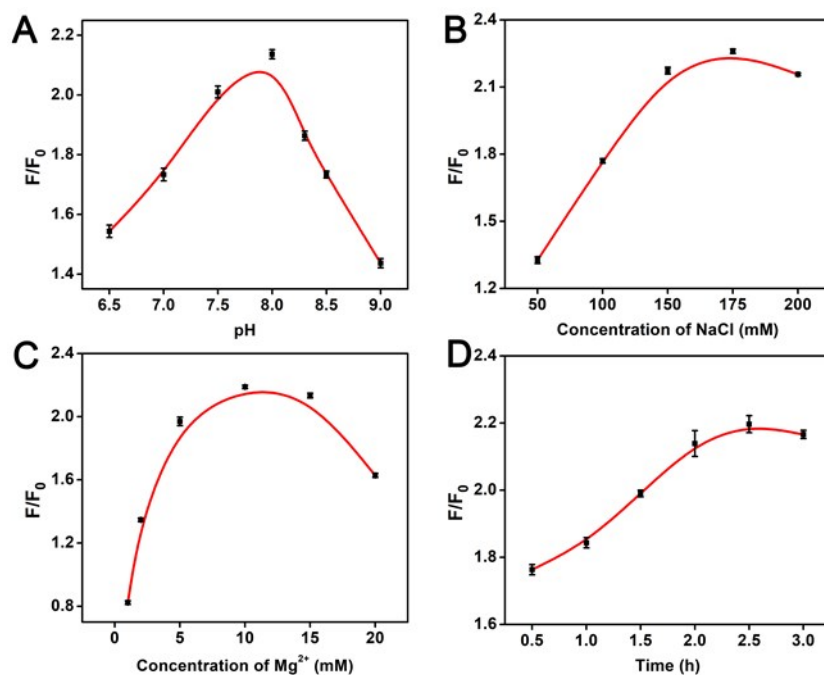


Fig. S9 Optimization of the control nanoprobe reaction condition, in which the curves are drawn based on the spline function method in the Origin software. (A) Effect of pH conditions on F/F_0 , and control nanoprobe. (B) Effect of NaCl concentration on F/F_0 . (C) Effect of Mg^{2+} concentration on F/F_0 . (D) Effect of reaction time on F/F_0 .

The reaction conditions of the control molecular beacon and the control nanoprobe,

including the pH, the concentration of sodium, the concentration of magnesium and the reaction time, are optimized. The value of F/F_0 is adopted to appraise the performance of the control systems, where F and F_0 are fluorescence signal responses of control systems in the presence and absence of target sequence, respectively. The goal of optimization is to improve the F/F_0 , so as to obtain the best performance for the control systems. For the control molecular beacon, the optimized pH value is 8.3. The appropriate concentrations for NaCl and Mg^{2+} are 150 mM and 10 mM respectively, and the proper reaction time is 1.0 h (Fig. S8). For the control nanoprobe, the optimized pH value is 8.0. The appropriate concentrations for NaCl and Mg^{2+} are 175 mM and 10 mM respectively, and the proper reaction time is 2.5 h (Fig. S9).

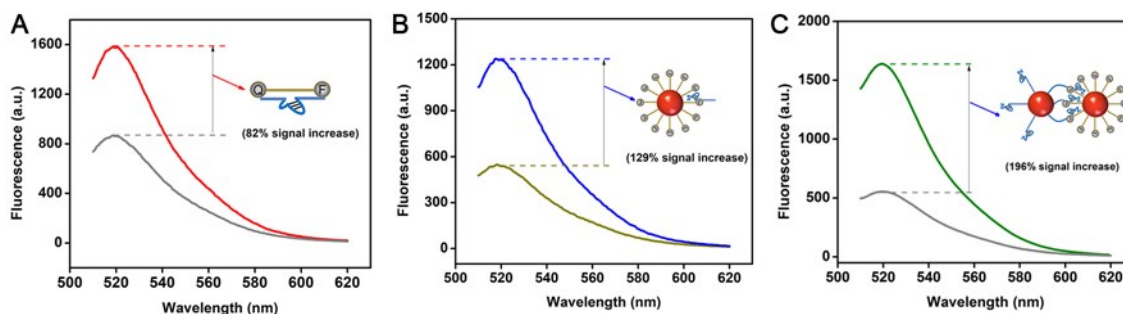


Fig. S10 Fluorescence emission spectra of the control molecular beacon (A), control nanoprobe (B) and interparticle relatively motional DNA walker (C).

Under the optimal conditions of each system, the fluorescence characterization of DNA walker, the control molecular beacon and the control nanoprobe with or without target were carried out. As shown in Fig. S10, the signal increase of the DNA walker is superior to that of the two control systems.

The DNA walker shows a strong fluorescence response with 196% signal growth. However, the control molecular beacon shows merely 82% signal growth with a relatively high background. The high background is due to the fact that the quencher may not quench fluorescence of fluorescent dyes completely.³ It has been reported that the background can be reduced by increasing the number of quencher on molecular beacon, but it will weaken the binding between the DNAzyme and substrate, and the label might also interfere with a functional DNA as it interacts with its targets,⁴⁻⁷ which are not very effective for improving the

signal growth. Compared to the control molecular beacon, the control nanoprobe exhibits 129% signal growth with a lower background. This is due to the good quenching ability of AuNPs and the higher binding constant of nanoparticle probes to combine free oligonucleotides, so the DNA strand hybridization on the nanoparticle probe surface is better than in solution.⁸ The control nanoprobe shows weaker signal growth compared to the DNA walker composed of WP and TP. The hybridization efficiency of DNA and DNA functionalized-AuNPs is limited, for example, it is reported in the literature that the hybridization efficiency of oligonucleotide-modified nanoparticles to DNA strands is limited,⁹ and the hybridization of free DNA strands to DNA functionalized AuNPs occurs with negative cooperativity.¹⁰ In contrast, the melting properties of DNA-linked AuNPs assemblies exhibit the cooperation effect between DNA-AuNPs.¹¹ Therefore, the binding of WP and TP is better than that of DNA strands to DNA-AuNPs due to the cooperation effect. And the multivalent interaction between WP and TP could be formed under the cooperation effect, which improves the kinetics and fluorescence enhancement. In addition, AuNPs of WP and TP have strong spatial effect and high ionic charge, which can be used to effectively stabilize DNA.¹² The good stability of WP and TP is beneficial to the application of DNA walker in real samples analysis.

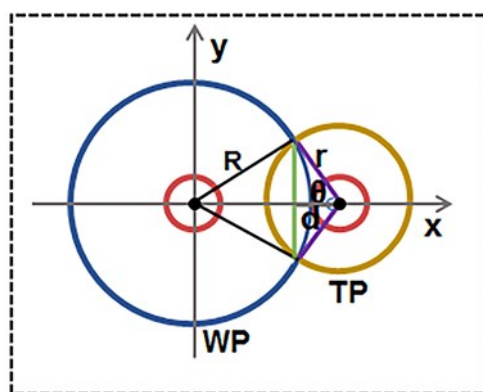


Fig. S11 Schematic diagram of the calculation model.

The calculation process of the distance from TP center to common chord (d) is as follows: a plane rectangular coordinate system is established with the center of the WP circle as the dot (Fig. S11). Therefore, according to the coordinate of circle center (0, 0) and radius of WP ($R = 29.9 \text{ nm}$), the equation of WP circle is:

$$x^2 + y^2 = 29.9^2;$$

in which x and y represent the horizontal and vertical coordinates of any point on the WP circle.

According to the coordinate of circle center (36.4, 0) and radius of TP ($r = 17.7$ nm), the equation of TP corresponding circle is:

$$(x-36.4)^2 + y^2 = 17.7^2;$$

in which x and y represent the horizontal and vertical coordinates of any point on the TP circle.

Since the WP and TP circles are overlapped to generate two intersection points, which satisfy the equations of both WP and TP circles, as well as the equation by subtracting equation of WP circle from equation of TP circle. Therefore, the equation after subtraction is the linear equation that is applicable to both intersection points, which is the common chord equation when two circles intersect:

$$(x^2 + y^2) - [(x-36.4)^2 + y^2] = 29.9^2 - 17.7^2.$$

After calculation, $x = 26.1$. It means that the distance from any point the common chord to the y-axis is 26.1 nm.

Thus, the distance between the center of WP circle and the common chord is 26.1 nm. Combining the distance between the centers of two circles (36.4 nm), it can be calculated that the distance from TP center to common chord is: $d = 36.4 \text{ nm} - 26.1 \text{ nm} = 10.3 \text{ nm}$.

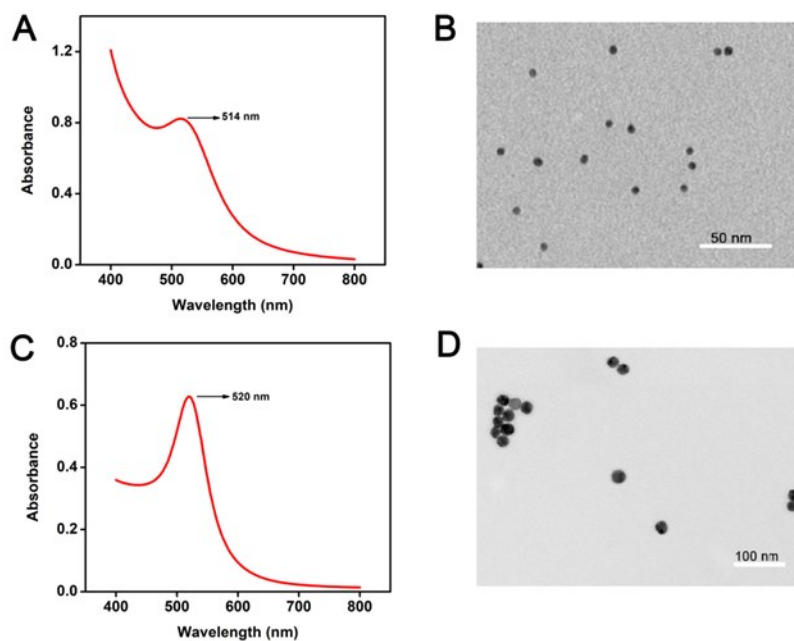


Fig. S12 Characterization of 5 nm and 25 nm AuNPs. (A) UV-vis spectra of 5 nm-AuNPs and (B) TEM image of 5 nm-AuNPs. (C) UV-vis spectra of 25 nm-AuNPs and (D) TEM image of 25 nm-AuNPs.

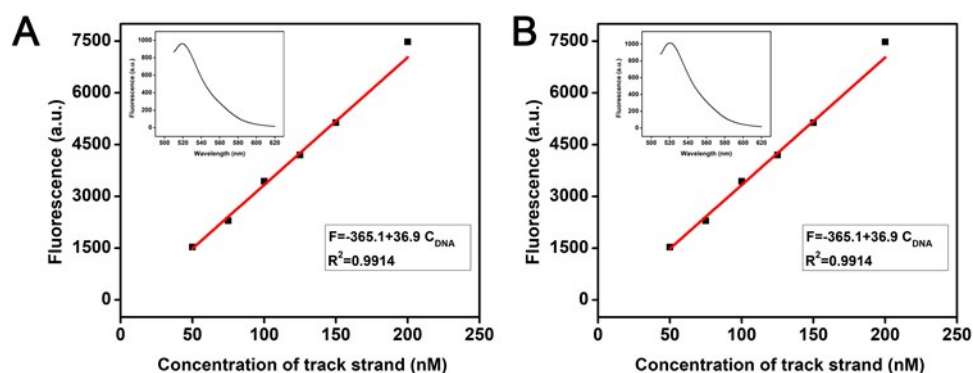


Fig. S13 Characterization of the modified amount of TP-Au5 and TP-Au25. (A) Standard linear calibration curves of FAM-labelled track strand. Inset shows the fluorescence spectra of TP-Au5 after incubation with DTT. (B) Standard linear calibration curves of FAM-labelled track strand. Inset shows the fluorescence spectra of TP-Au25 after incubation with DTT. The Error bars are the standard deviation of three measurement.

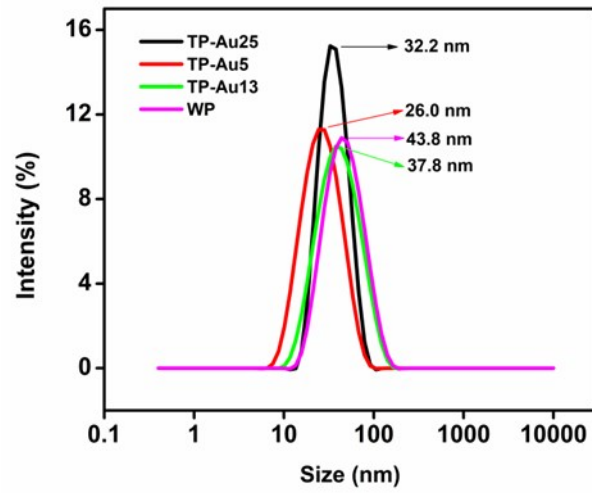


Fig. S14 DLS characterization of WPs and different sizes of TPs.

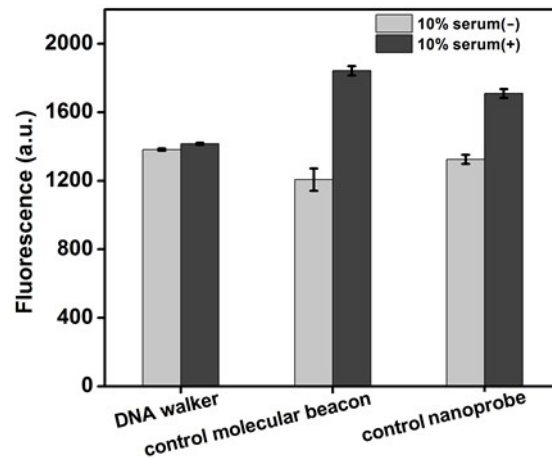


Fig. S15 Comparison of anti-interference ability of the interparticle relatively motional DNA walker, control molecular beacon and control nanoprobe.

Additional tables.

Table S1. Comparison of the DNA walker with some reported strategies for ZIKV related sequence.

Detection technique	Assay strategy	Target	Detection limit	Real sample matrix tested	Ref
Fluorescence	Three-dimensional metal-organic framework (MOF) based reaction assay	Zika virus RNA	192 pM	No	13
Fluorescence	Nitrogen-doped porous carbon-based fluorescence sensor	Zika virus RNA	230 pM	Saliva sample	14
Fluorescence	Two-dimensional MOF of [Cu(Dcbb)(bipy)(OH)]n-based fluorescence sensor	Zika virus RNA	200 pM	No	15
Electrochemical	Label-free electrochemical DNA biosensor	Zika virus complementary	25 nM	No	16
Electrochemical	Graphene-enabled Zika biosensor	Zika virus RNA (NS1)	450 pM	Human blood serum	17
Fluorescence	An interparticle relatively motional DNA walker based fluorescence analysis	Zika virus RNA	118 pM	Human blood serum	This work

Table S2. Recovery experiment of ZIKV-RNA in human serum.

Sample	Actual concentration (nM)	Measured concentration (nM) ^a	recovery (%)	RSD (%)
1	2.0	2.0	100.0%	5.0%
2	8.0	7.8	97.5%	3.8%
3	14.0	14.5	103.5%	1.4%

^aAverage of three parallel experiments

Table S3. The sequences of DNA and RNA used in this study. The blue regions of walking strand and DNazyme strand represent the catalytic sequence of the 8-17E DNazyme. The rA in red of track strand and substrate strand denotes adenosine ribonucleotide.

Name	Sequence (5'→3')
	HS-
Walking strand	(T) ₂₈ TGGGAAAGACTCTCTTCTCCGAGCCGGTCGAAATAGTGC
	GT
Locking strand	AAGAGAGTCTTTCCCACGTCAATATGCT
Track strand	HS-(T) ₁₄ ACGCACTATrAGGAAGAGAT-6-Carboxyfluorescein(FAM)
Target RNA of ZIKA	AGCAUUAUUGACGUGGGAAAGAC
T-DENV	UGGUGCUGUUGAGUCAACAGGUUCU
T-JEV	UGUAGCUGGUGGUGAGGAAGAACAC
T-YFV	UUUGGAUGAAAAACACAAAACCACU
DNazyme strand	TGGGAAAGACTCTCTTCTCCGAGCCGGTCGAAATAGTGCGT
Substrate strand	FAM-ACGCACTATrAGGAAGAGAT-BHQ1

References

(1) M. Cepeda-Plaza, C. E. McGhee and Y. Lu, *Biochemistry*, 2018, **57**, 1517-1522.

- (2) W. H. Zhou, R. Saran and J. W. Liu, *Chem. Rev.*, 2017, **117**, 8272-8325.
- (3) W. C. Xu and Y. Lu, *Anal. Chem.*, 2010, **82**, 574-578.
- (4) J. W. Liu and Y. Lu, *Anal. Chem.*, 2003, **75**, 6666-6672.
- (5) T. Lan, K. Furuya, and Y. Lu, *Chem. Commun.*, 2010, **46**, 3896-3898.
- (6) Y. Xiang, Z. D. Wang, H. Xing, N. Y. Wong and Y. Lu, *Anal. Chem.*, 2010, **82**, 4122-4129.
- (7) Y. Xiang, A. J. Tong and Y. Lu, *J. Am. Chem. Soc.*, 2009, **131**, 15352-15357.
- (8) A. K. R. Lytton-Jean and C. A. Mirkin, *J. Am. Chem. Soc.*, 2005, **127**, 12754-12755.
- (9) L. M. Demers, C. A. Mirkin, R. C. Mucic, R. A. Reynolds, R. L. Letsinger, Robert Elghanian and G. Viswanadham, *Anal. Chem.*, 2000, **72**, 5535-5541.
- (10) P. S. Randeria, M. R. Jones, K. L. Kohlstedt, R. J. Banga, M. O. d. I. Cruz, G. C. Schatz and C. A. Mirkin, *J. Am. Chem. Soc.*, 2015, **137**, 3486-3489.
- (11) R. C. Jin, G. S. Wu, Z. Li, C. A. Mirkin and G. C. Schatz, *J. Am. Chem. Soc.*, 2003, **125**, 1643-1654.
- (12) Y. C. Shiang, C. M. Ou, S. J. Chen, T. Y. Ou, H. J. Lin, C. C. Huang and H. T. Chang, *Nanoscale*, 2013, **5**, 2756-2764.
- (13) B. P. Xie, G. H. Qiu, P. P. Hu, Z. Liang, Y. M. Liang, B. Sun, L. P. Bai, Z. H. Jiang and J. X. Chen, *Sensor. Actuator. B Chem.* 2018, **254**, 1133-1140.
- (14) J. Li, K. Yang, Z. Wu, X. D. Li and Q. Y. Duan, *Talanta*, 2019, **205**, 120091.
- (15) B. P. Xie, G. H. Qiu, B. Sun, Z. F. Yang, W. H. Zhang, J. X. Chen and Z. H. Jiang, *Inorg. Chem. Front.* 2019, **6**, 148-152.
- (16) H. A. M. Faria and V. Zucolotto, *Biosens. Bioelectron.* 2019, **131**, 149-155.
- (17) S. Afsahi, M. B. Lerner, J. M. Goldstein, J. Lee, X. L. Tang, D. A. Bagarozzi Jr., D. Pan, L. Locascio, A. Walker, F. Barron and B. R. Goldsmith, *Biosens. Bioelectron.* 2018, **100**, 85-88.